Advances in Geo-Energy Research

Vol. 14, No. 2, p. 147-160, 2024

Original article

Development and validation of a remotely triggered pressure- and gas-preserved coring tool for deep coal mines in drilling fluid environments

Ju Li[1,3], Jianan Li[2,3]*, Tianyu Wang[2,3], Xiaojun Shi[2,3], Pengfei Cui[4,5], Delei Shang[4,5]

[1]*School of Mechanical Engineering, Sichuan University, Chengdu 610065, P. R. China*

[2]*College of Water Resource and Hydropower, Sichuan University, Chengdu 610065, P. R. China*

[3]*State Key Laboratory of Intelligent Construction and Healthy Operation and Maintenance of Deep Underground Engineering, Sichuan University, Chengdu 610065, P. R. China*

[4]*State Key Laboratory of Intelligent Construction and Healthy Operation and Maintenance of Deep Underground Engineering, Shenzhen University, Shenzhen 518060, P. R. China*

[5]*Guangdong Provincial Key Laboratory of Deep Earth Sciences and Geothermal Energy Exploitation and Utilization, Shenzhen University, Shenzhen 518060, P. R. China*

Keywords:
Deep coal mine
pressure- and gas-preserved coring
remote coring trigger device
shear force calculation
drilling fluid environment

Cited as:
Li, J., Li, J., Wang, T., Shi, X., Cui, P., Shang, D. Development and validation of a remotely triggered pressure- and gas-preserved coring tool for deep coal mines in drilling fluid environments. Advances in Geo-Energy Research, 2024, 14(2): 147-160.
https://doi.org/10.46690/ager.2024.11.07

Abstract:
The accurate measurement of coal seam gas content is essential for several aspects of deep coal mining, including disaster management, resource allocation and sustainability. However, obtaining *in-situ* coal samples while preserving gas content under challenging conditions, such as high stress, temperature fluctuations, and drilling fluid environments, remains a significant challenge. To overcome this difficulty, we present an innovative *in-situ* pressure- and gas-preserved coring tool specifically designed for deep coal mining applications. This device enables the collection of coal seam samples under *in-situ* conditions while ensuring that both pressure and gas content are preserved, thereby preventing gas escape during sample transfer and providing more accurate parameters for evaluating coal and natural gas reserves. In the demanding environment of deep coal seams, the performance of the pressure-preserved chamber of the corer relies on the reliability of its remote triggering mechanism. The presence of drilling fluid introduces medium resistance, which can impair the triggering process–an issue largely overlooked in previous research. Herein, we propose a robust method to calculate remote triggering forces within liquid media and optimize its key parameters to improve operational stability. Laboratory tests and field validations in coal mining environments are conducted, which confirm the effectiveness of the optimized design and demonstrate the tool's practical applicability. This study offers valuable insights into addressing key challenges in deep coal reservoir exploration and gas resource preservation.

1. Introduction

Energy serves as the propelling force for swift socio-economic advancement, with coal playing a pivotal role in national energy frameworks (Ma et al., 2021). Gas, being a substantial unconventional resource within coal mines, is often associated with safety concerns such as gas explosions and outbursts (Baouche and Wook, 2020). Therefore, the precise measurement of gas holds immense importance for

Yandy Scientific Press

*Corresponding author.
E-mail address: liju1@stu.scu.edu.cn (J. Li); lijianan@scu.edu.cn (J. Li); scuwty@163.com (T. Wang); Shixiaojun@stu.scu.edu.cn (X. Shi); cpf6134@163.com (P. cui); sdl18@tsinghua.org.cn (D. Shang).

Received September 13, 2024; revised October 7, 2024; accepted October 29, 2024; available online November 4, 2024.

disaster prevention, energy management, and the facilitation of environmentally sustainable coal mining practices. Gas in-place estimation is crucial for coalbed methane development, with direct measurement being the prevalent method (Bertard et al., 1970; Saghafi, 2017). This approach involves summing loss gas, measured gas from samples, and measured residual gas from crushed coal (Wang et al., 2015). Gas loss, occurring during sample lifting and exposure, is challenging to measure directly. Some scholars utilize the square root time method (Yee et al., 1993; Li et al., 2019a), while errors may arise due to idealized estimation models and uncertainties. The time-intensive deep hole coring method results in a notable dissipation of loss gases from the coal sample, thereby compromising the accuracy of total gas content measurements. Therefore, it is essential to effectively minimize gas leakage during the core extraction process to ensure more precise gas content values in coalbed methane exploration.

To address the above challenge, sealed coring technology has been proposed, sealing coal samples at the hole's bottom to prevent free gas escape during lifting and ground exposure, eliminating errors arising from inaccurate loss estimation (Sun et al., 2020). To this end, the freezing core sampling technique (FCST) (Wang et al., 2015) has yielded excellent results. Closed-core sampling yields accurate gas content results but alters the *in-situ* environment, affecting pressure. Therefore, Huang et al. (2023) proposed the principle of the low-disturbance pressure-preserving corer, introducing new equipment for precise gas content measurement. This principle emphasizes the importance of effectively maintaining the *in-situ* conditions of coal samples for the accurate determination of coal reserve evaluation parameters. Sun et al. (2020) proposed a device for coring and measuring gas content in coal seams through underground boreholes, achieving higher gas content than conventional coring.

Acquiring *in-situ* coal samples from deep coal seams and ensuring the stable sealing of pressure chambers present significant challenges due to the harsh underground coring conditions, limited space, and the complex solid-liquid environment created by the mixing of drilling fluid and coal debris. As such, the specific challenges in obtaining deep *in-situ* coal samples include the following:

1) Collecting coal samples in complex *in-situ* environments (characterized by high pressure and fluid interactions) and preserving *in-situ* pressure and the state of gas occurrence.
2) Presenting a reliable method to remotely transition from precise core collection to pressure-preserved storage under harsh conditions.

Firstly, the design of the pressure chamber is crucial, as the performance of the chamber structure determines the upper limit pressure of the equipment's working environment. The pressure chamber design also needs to consider the movement process of core recovery, making it a complex and time-consuming structural design. Usually, the pressure chamber includes seals at the upper end, lower end and side walls, and the side wall seal is usually composed of the outer tube of the core extractor. Earlier systems, such as the pressure core barrel used in the Deep Sea Drilling Program, utilize a combination of energy storage devices and one-way valves to control upper-end pressure retention (Kvenvolden and Cameron, 1983). The pressure core sampler, the primary sampling tool for the International Ocean Discovery Program, achieves upper-end sealing through ball throwing (Abid et al., 2015; Dickens et al., 1997, 2003). The Fugro pressure core relies on an internal hydraulic impact mechanism for penetrating core extraction and achieves upper-end sealing by rotating the seal (Schultheiss et al., 2006, 2009). However, using pitching for an upper seal may lead to instability due to ball displacement, and combining impact structure with sealing significantly increases design complexity. The pressure temperature coring system developed by the Japan National Oil Corporation employs a ball valve to seal the lower end and a separated rotary dynamic seal to form a pressure-preserved chamber (He et al., 2020; Masayuki et al., 2006). The MeBo pressure vessel system, developed in Germany for integration with underwater drilling rigs, utilizes a rope mechanism to trigger the bottom flap valve controller, combined with a rotating dynamic seal at the upper end, to achieve sealing at both the upper and lower ends (Pape et al., 2017). Li et al. (2022) analyzed the influence of micro-surface characteristics of materials on the surface contact of flap valves to guide the sealing design of pressure retaining systems. Li et al. (2021)'s newly proposed saddle pressure-preserved controller boasted an ultra-high pressure-bearing capacity, surpassing 100.9 MPa. A deep *in-situ* coring system, equipped with a pressure-preserved controller capable of withstanding an ultimate bearing capacity exceeding 140 MPa, was used to acquire *in-situ* rock core specimens from deep underground (Xie et al., 2023). These pressure-preserved coring devices have achieved certain success in various fields, but still face stability and reliability issues during the process of switching to the pressure-preserved state after coring is completed.

Secondly, deep coal seams are situated in complex environments characterized by high temperature, high water pressure, high stress, and multi-phase coupling, where the presence of various media such as drilling fluid, gas and coal solids at the coring point significantly impacts the success rate of remote triggering (Xie et al., 2023, 2024). Specifically, the drilling fluid environment in deep coal mines not only has a beneficial effect on lubricating and chip removal during the *in-situ* coring of coal seams but also fluid incompressibility has negative effects in some cases under limited space conditions. Moreover, horizontal holes at 100 m depth are not perfectly horizontal; their trajectory is influenced by gravity (Mahmoud et al., 2020). The end of these holes often contains a liquid medium, primarily water mixed with coal debris. While the use of drilling fluid helps to clean the cuttings in the well, reduce frictional resistance and torque, and reduce the risk of pipe blockage (Mahmoud et al., 2020), the closure of the critical lower end seal (pressure-preserved controller) requires sufficient time and stroke, which necessitates the remote triggering mechanism to complete the pressure-preserved action within the designed stroke. However, the resistance of the liquid medium has a significant impact on achieving the triggering stroke, which phenomenon has not been thoroughly studied.

Table 1. Comparison of key parameters in coring technologies applied to the coal and oil industries.

Scope	Name	Pressure capacity (MPa)	Drilling diameter (mm)	Sample diameter (mm)	Equipment length (mm)
Coal	Sealed corer (Sun et al., 2020)	10	130	38	2,150
	GW-CP194-80M (Zhu et al., 2020)	20	215.9	80	6,000
	PH core drilling tool (Li et al., 2019b)	20	215.9	85	-
	PGP-Coring tool (Proposed)	25	122	50	1,900
Oil & gas	GW-CP194-80A (Yang et al., 2020)	60	215.9	80	8,000
	IPP-Coring tool (Guo et al., 2024)	70	215	50	6,800
	IPCS (Li et al., 2024)	30	215.9	50	5,300
	DAPC (Abegg et al., 2008)	20	450	84	7,000

To address the aforementioned challenges, this study designed a new remotely triggered pressure- and gas-preserved coring (PGP-Coring) tool specifically designed for deep coal mining applications. This innovative tool is capable of extracting coal samples with a diameter of 50 mm and a maximum length of 500 mm under complex downhole conditions. The device maintains environmental pressures of up to 8 MPa during storage and transport, effectively reducing the risk of gas leakage and ensuring the integrity of samples for subsequent parameter analysis. In addition, to achieve stable triggering from core collection to pressure storage, a detailed analysis was conducted using Coupled Euler-Lagrange (CEL) simulation, focusing on the relationship between triggering resistance, triggering velocity, medium density, and other factors. This facilitated the optimization of critical design parameters and the validation of strength criteria for the remote triggering mechanism. Finally, tests were performed, that demonstrated stable pressure retention of the PGP-Coring tool for 8 hours at 8 MPa, successfully obtaining *in-situ* pressurized coal samples from a depth of 700 m, with a horizontal sampling reach of up to 120 m.

2. Remotely triggered PGP-Coring tool for deep coal mines

Pressure-preserved coring technology (Schultheiss et al., 2006) first appeared in the field of petroleum and natural gas hydrates. Meanwhile, in the field of coal and coalbed methane development, coal seams have relatively shallow occurrence and are characterized by low reservoir pressure, low coal body strength, and different geological features and practical needs. Pressure-preserved coring equipment in the oil and gas field, such as the *in-situ* pressure-preserved coring (IPP-Coring) tool (Guo et al., 2024) and GW-CP194-80A (Yang et al., 2020), usually have high pressure resistance, large length and mass due to the great depth of the target coring layer. Thus, the supporting equipment such as drill bits need to be strictly adapted to the target formation, as shown in Table 1. Coal seam, on the other hand, has different requirements for the pressure-bearing capacity of the pressure-preserved coring equipment according to the depth of burial. For the development of coalbed methane, the Sealed Corer (Sun et al., 2020), GWCP194-80M (Zhu et al., 2020) and pressure holding (PH) core drilling tool (Li et al., 2019b) are surface drilling cores capable of depths exceeding 1,000 m, hence they have higher pressure-bearing capacity. In contrast, ground coring can be constructed using equipment such as towers, while underground tunnels have significant limitations regarding the use and operation of equipment due to the confined space, requiring the equipment to meet both requirements of sampling and ease of operation. For this purpose, we have designed the PGP-Coring tool to be suitable for tunnels. Compared to the Sealed Corer (Sun et al., 2020), the proposed PGP-Coring tool, owing to its superior internal pressure-preserved structure, enables sample extraction at comparable drilling diameters with a standard core diameter of 50 mm and offers a maximum pressure-bearing capacity of 25 MPa (Huang et al., 2023).

In general, the calculation of gas content needs to account for three components: Lost gas, measured desorption gas, and measured broken desorption gas. The primary difference between the USBM method and the pressure-preserved coring method for determining gas content lies in the calculation of lost gas (Diamond and Schatzel, 1998). In the USBM, the volume of gas released during the first ten hours of desorption is proportional to the square root of time, providing a basis for estimating the lost gas in coal samples recovered from vertical wells (Li et al., 2020). This method is widely applicable to estimating the lost gas content in oil shale, coal, and other

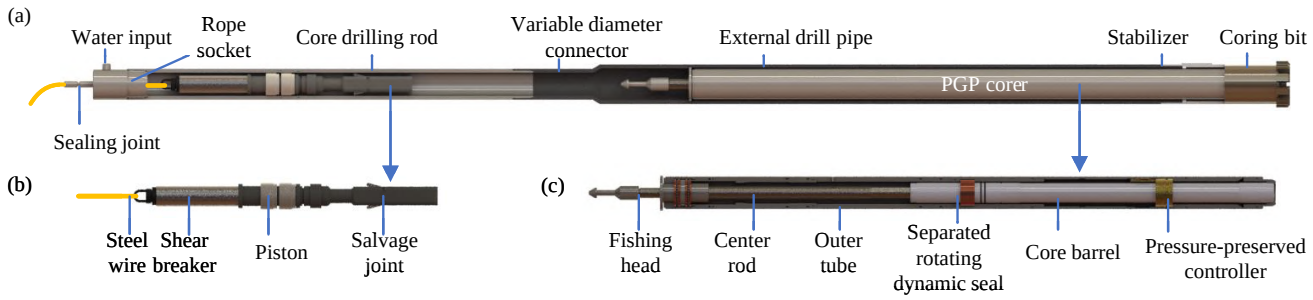

Fig. 1. Schematic diagram of the proposed PGP-Coring tool. (a) Structural overview of the PGP-Coring tool, (b) remote triggering mechanism of the salvage tool and (c) the PGP corer designed for coal sample collection and storage.

rock samples; however, its accuracy depends heavily on the alignment between the fitting function and field data, which can introduce estimation errors. In contrast, the pressure-preserved coring method prevents gas leakage during coal sample transfer, eliminating the need for algorithms to estimate lost gas, thereby reducing errors and improving the reliability of gas content measurements. Compared with conventional coring, the coalbed methane content determined using the pressure-preserved coring method is 20% to 30% higher (Sun et al., 2020).

The primary technical specifications of the PGP-Coring tool include a total length of 1,900 mm, an outer diameter of 114 mm, a drill bit diameter of 122 mm, a maximum core length of 600 mm, a core diameter of 50 mm, and a pressure-bearing capacity of up to 25 MPa, with lifting and lowering operations facilitated by standard drilling equipment. Moreover, the technology presented in this study is characterized by a lightweight design and ease of operation, offering potential applications for the cost-effective development of oil and gas fields and aiding the exploration of coalbed methane resources.

2.1 Equipment subcomponents

The proposed *in-situ* PGP-Coring tool is designed to extract pressure- and gas-preserved coal samples from deep coal seams while maintaining the original gas occurrence state of the coal body, as illustrated in Fig. 1. The tool incorporates dedicated drill rods for torque transmission and acquiring coal samples, a salvage tool for remote triggering, and a pressure- and gas-preserved corer (PGP corer) for obtaining and storing pressure-preserved coal samples.

The main components of the dedicated core drilling rod include a rope socket, core drilling rods, a variable diameter connector, an external drilling pipe, a stabilizer, and a coring bit, as shown in Fig. 1(a). The rope socket ensures the passage of a 5 mm diameter steel wire rope while maintaining a certain sealing capacity, and can be connected to a pressurized water source or an underground water pump at the sidewall opening. The outer diameter of the core drilling rod is 89 mm, and the inner diameter is 67 mm.

The salvage tool primarily comprises a steel wire rope, a shear breaker, a piston, and a salvage joint, as shown in Fig. 1(b). The function of the steel wire rope is transmitting tension. The design of the shear breaker is such that it allows transmitting axial tension through its internal shear pin that fractures when the safety threshold is exceeded. This threshold setting depends on the maximum resistance experienced by the separated rotating dynamic seal (SRDS). This controlled fracture results in the separation of the upper and lower parts of the shear breaker, disconnecting the axial tension transmission between the wire rope and the salvage tool.

The PGP corer comprises the key components of fishing head, center rod, SRDS, core barrel, pressure-preserved controller, and the outer tube of the corer, as shown in Fig. 1(c). The fishing head is equipped with a conical structure for connecting the salvage joint, and the axial tension is transmitted through the center rod to unlock the axial movement of the core barrel, allowing it to be lifted. Upon reaching the designated position, the SRDS achieves sealing at the upper end of the pressure-preserved chamber. Simultaneously, the pressure-preserved controller's limit is released to accomplish sealing at the lower end of the pressure chamber. The SRDS plays a crucial role in the initial positioning of the core barrel, preventing axial movement during drilling to safeguard the integrity of the core. Additionally, it forms a dynamic seal with the outer tube after triggering movement. The primary functions of the outer tube include sealing the side walls of the pressure chamber, maintaining the relative positions of internal components within the entire system, and upholding the overall structural strength of the tool.

2.2 Workflow and failure mechanism

In order to fully understand the working process and failure forms of the PGP corer, a detailed schematic diagram of the entire process of the PGP coring tool was shown in Fig. 2. The workflow mainly includes *in-situ* coring and remote triggering. The brief description of each step is as follows:

1) Pre-drilling Underground: Use a 130 mm diameter drill bit for drilling to the specified position. Subsequently, remove the drilling tool in readiness for core drilling operations.
2) Lowering the PGP corer: Insert the PGP corer into the external drill pipe with a diameter of 114 mm. Connect the external drill pipe to a dedicated corer drilling rod (89 mm diameter) through a variable-diameter connector. Employ a drilling rig to progressively lower a sequence of specialized corer drill rods (each with 89 mm diameter) to the predetermined target position, as illustrated in Fig.

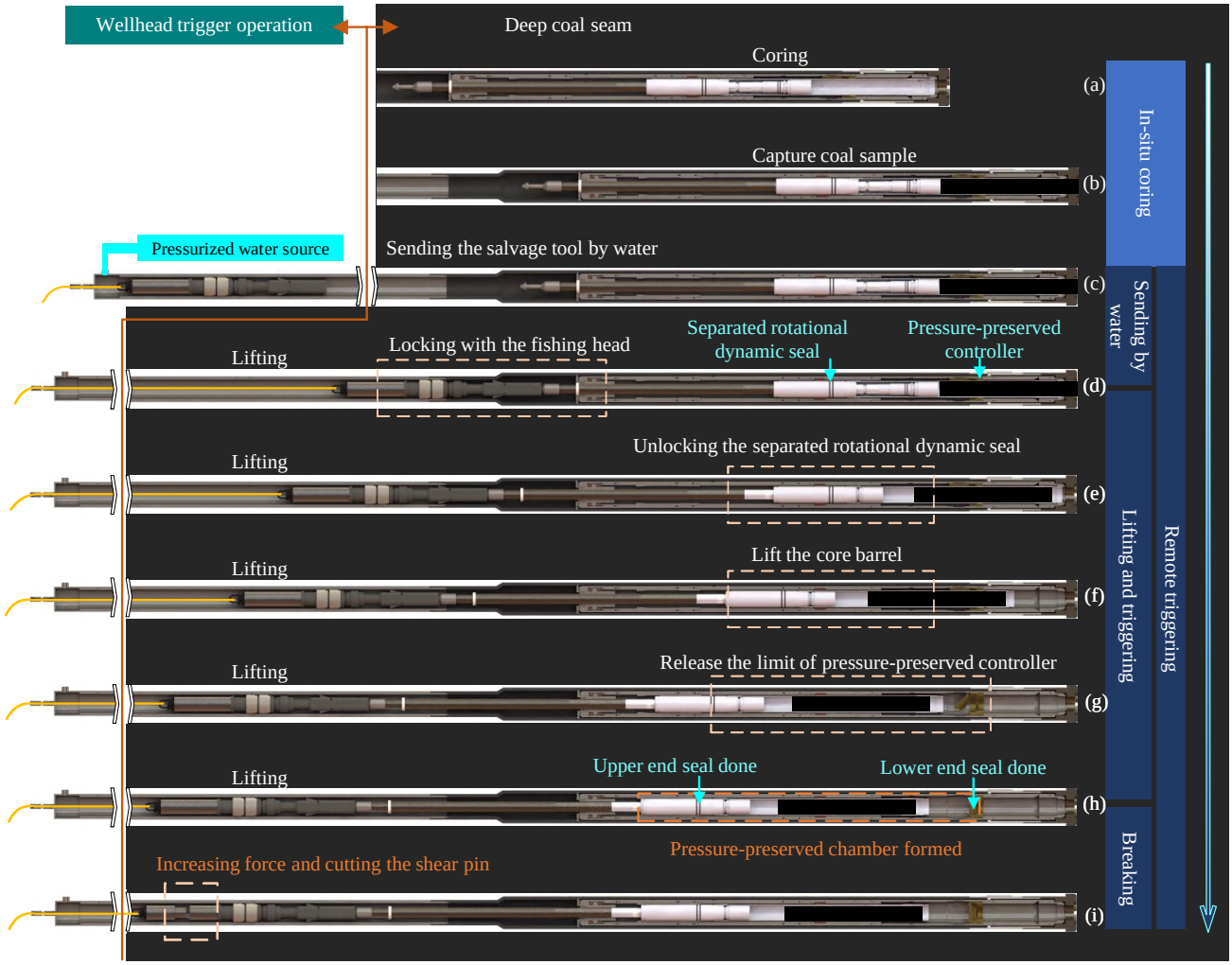

Fig. 2. Schematic diagram of remote triggering workflow for the proposed PGP-Coring tool. (a) Lower the corer to the specified depth, (b) obtain coal samples, (c) install the salvage tool, (d) lower the salvage tool, (e) unlock the SRDS, (f) lift the core barrel, (g) release the pressure-preserved controller's limit, (h) create a pressure-preserved space inside the PGP corer and (i) cut the shear pin.

2(a).

3) Drilling of Coal Core: After reaching the hole bottom, conduct drilling at a depth of 650 mm with a minimal water flow rate, low drilling pressure, and reduced rotation speed. Allow the entire coal core to enter the barrel, as depicted in Fig. 2(b).
4) Lowering the Salvage Tool: Substitute the rope socket and insert the salvage tool, connected to the steel wire rope, into the dedicated core drilling rod, as shown in Fig. 2(c).
5) Preparation for Triggering Action of the PGP corer: Utilize water pressure to guide the salvage tool to the hole bottom, connecting and securing it with the fishing head at the PGP corer's upper end, as depicted in Fig. 2(d).
6) Corer Triggering: This multi-step process involves tension transmission through the steel wire rope.

Step 1: Move the center rod by a predetermined safe distance under tension, unlocking the SRDS, as shown in Fig. 2(e).

Step 2: Lift the core barrel as it enters the designated pressure chamber, as depicted in Fig. 2(f).

Step 3: During lifting, the lower end of the core barrel passes through the pressure-preserved controller, releasing its limit and achieving self-triggering sealing under elasticity/magnetic force, as shown in Fig. 2(g).

Step 4: Continue lifting while the SRDS combines with the outer pipe, forming an upper-end seal, as shown in Fig. 2(h).

Step 5: Increase tension further, cut shear pins in the salvage tool, sever power transmission, and complete the triggering process, as illustrated in Fig. 2(i).

7) Core Retrieval: Extract the complete set of the PGP-Coring tool, dismantle the PGP corer, place it into a designated tool transportation box, and move it to the ground.

The tool application scenario proposed in this article is underground sampling in deep coal mines with a vertical depth

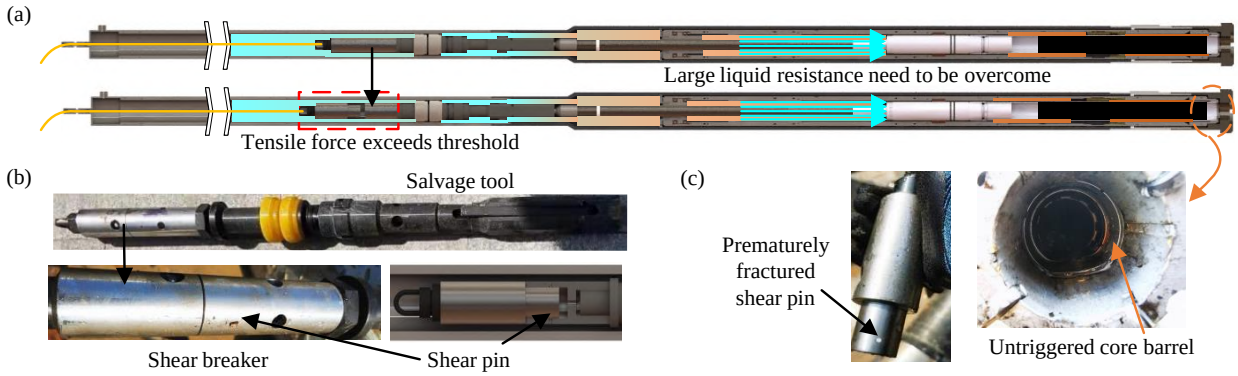

Fig. 3. Schematic diagram of remote triggering failure of the proposed PGP-Coring tool. (a) The failure step occurs at the beginning of the upward triggering mechanism, (b) image of the physical object of the salvage tool and the installation position of the shear pin and (c) the shear pin was cut in advance without normal triggering and the core barrel was not lifted.

greater than 600 m. Coal seams at this depth typically have high initial gas pressure and gas content. If the *in-situ* gas pressure can be successfully preserved, gas leakage can be effectively avoided during sample transfer, thereby improving the accuracy of reserve assessment. However, when extracting coal cores from downward boreholes with depths exceeding 60 m, drilling fluid (usually clean water from underground coal mines) accumulates in the borehole. The presence of this liquid medium creates resistance to the movement of the sealing components, significantly affecting the normal operation of the self-triggered sealing function of the corer triggering component.

As a key part of the sealing structure, the unlocking and movement of the SRDS are strongly affected by tension. The maximum transmitted tension depends on the shear strength of the shear pin. This is because the force transmission of the entire system needs to be achieved through shear pins, which are the weakest points. If its strength limit is exceeded, the pin will shear off and the force transmission will also be cut off. This in turn prevents the proper sealing of the upper and lower ends of the pressure chamber. Achieving a delicate balance in managing liquid medium resistance is crucial to preventing untimely shear pin failure and ensuring the effective functioning of the SRDS in sealing the pressure chamber, which is also the focus of this study. Fig. 3 shows the stages of failure after unlocking the SRDS step (i.e., Fig. 2(e)), along with images of the failed components, including the prematurely cut shear pins in the fishing device and the improper triggering of the core barrel. The physical diagram of the salvage tool and the schematic diagram of the shear breaker are presented in Fig. 3(b). As depicted in Fig. 3(c), laboratory testing reveals that due to the elevated liquid resistance surpassing the calculated required triggering force, the core barrel fails to ascend normally, resulting in failing to establish the pressure chamber.

The successful triggering of the PGP-Coring tool necessitates a tensile force that remains below the shear force of the shear pin. When operating under drilling fluid conditions, the triggering action involves the movement of a solid with an initial velocity in the fluid, resulting in significant fluid resistance. Consequently, the required tension is notably higher than that observed in experimental air environments. Therefore, the design tension of the PGP-Coring tool should comprehensively account for the impact of fluid resistance, guiding the selection of the shear pin. To address this need, a simulation calculation model based on the PGP-Coring tool was developed, with the aim to explore the influencing factors of fluid resistance.

3. Simulation analysis of liquid resistance

This article employs the finite element analysis method based on CEL to conduct a numerical simulation of the triggering process. This includes the exploration of the influence of various factors, such as initial pulling speed, medium density and object density, on the magnitude of fluid medium resistance.

3.1 Numerical model

Based on the proposed PGP corer, a hydraulic impact model of the triggering components is established, which incorporates the outer tube of the corer, the center rod, and the triggering structure (comprising the SRDS and core barrel). The dimensions of the outer tube are a diameter of 90 mm, inner diameter of 62.5 mm, and length of 1,700 mm. The center rod has a diameter of 36 mm and a length of 600 mm; the trigger structure has a diameter of 58 mm and a length of 1,000 mm, as depicted in Fig. 4(a).

Considering the intricate and diverse working environment of the PGP-Coring tool in coal mines, involving multiple fields and directions, material corrosion resistance and rust prevention ability are essential requirements. To meet these specifications, the outer tube, the center rod, and the trigger structure of the corer are all fabricated from 304 grade stainless steel material. The density parameters of 304 stainless steel are 8.0×10^{-9} t/mm^3, elastic modulus of 1.9×10^5 MPa, Poisson's ratio of 0.29, tensile strength of 823.6 MPa, and yield strength of 634 MPa. For the drilling fluid, common clean water in coal mines is selected, with a density of 1×10^{-9} t/mm^3. The liquid is intended to fill the gap area between the outer tube and the center rod of the corer, as well as the triggering

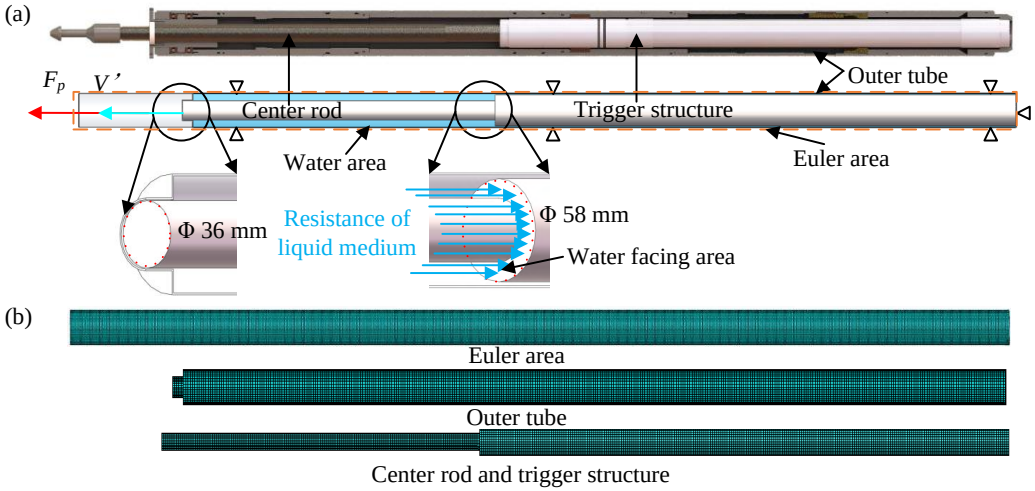

Fig. 4. Schematic diagram of the simulation model. (a) A hydraulic impact model for the triggering component of the PGP corer and (b) 3D mesh model of the PGP corer.

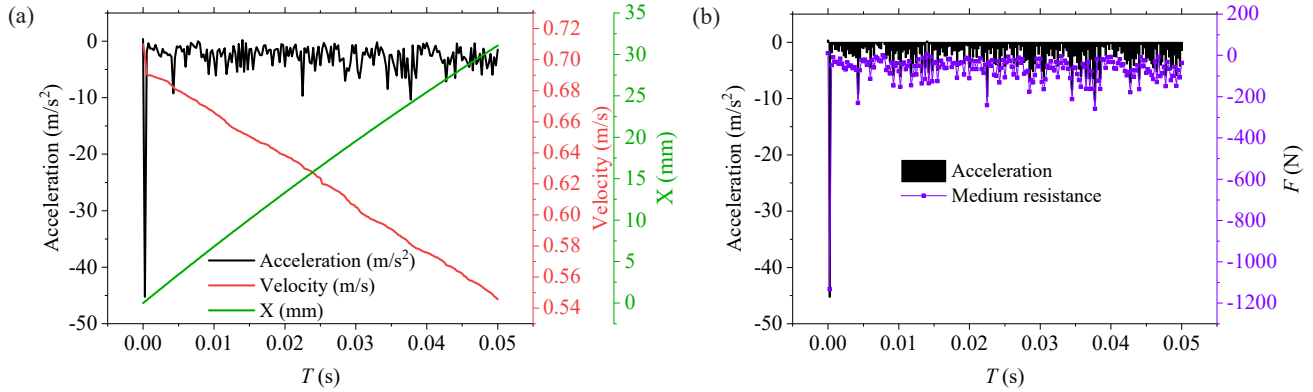

Fig. 5. In the scenario where the center rod and triggering structure have a speed of 0.71 m/s, the following information is provided: (a) The changes in acceleration, velocity and displacement and (b) the magnitude of the medium resistance, which was calculated based on the acceleration, with a maximum value of 1,179 N.

structure. To facilitate the CEL calculation, the Euler region needs to encompass the motion region of the liquid. Therefore, the diameter and length of the Euler region are set to 62.5 mm and 1,800 mm, respectively.

To streamline the calculations, considering the high yield strength of stainless steel, the outer tube, the center rod, and the trigger structure of the corer are treated as rigid bodies in the simulation. The center point of the upper-end face of the center rod is selected as the measuring point, and the velocity, acceleration, and displacement change curves of this measuring point are obtained through simulation. Taking into account the influence of gravity, liquid medium resistance, and pulling force on the component, subtracting the acceleration due to gravity and the pulling force allows for the determination of the magnitude of liquid medium resistance. Given the object's mass, the magnitude of medium resistance can be derived from the simulation results, as shown in Eq. (1) and Fig. 5.

$$F_p - (m_s + m)\,g - F_{mr} = (m_s + m)\,a \tag{1}$$

where F_p represents the magnitude of the pulling force, m_s represents the mass of the salvage tool, m represents the total mass of the center rod and trigger structure, F_{mr} represents the resistance of the medium, and a represents the acceleration along the direction of motion.

The surface stress cloud map depicted in Fig. 6(a) reveals that the predominant impact of liquid medium resistance is localized on the upper surface of the triggering structure. Furthermore, the force exerted on the center rod wall is oriented perpendicular to the direction of motion, therefore it is not taken into consideration. For grid independence testing, we examined the variation in maximum liquid resistance at an initial speed of 0.71 m/s and an initial tension of 250 N. As depicted in Fig. 6(b), when the number of grids surpasses 305,238, the rate of change in maximum resistance is 2.3%. Consequently, future experiments will adopt this grid configuration to ensure the independence of experimental results from grid variations.

3.2 Analysis of factors influencing medium resistance

Building upon fundamental knowledge in fluid mechanics and the structural design of the corer, this article identifies three primary influencing indicators to analyze factors affect-

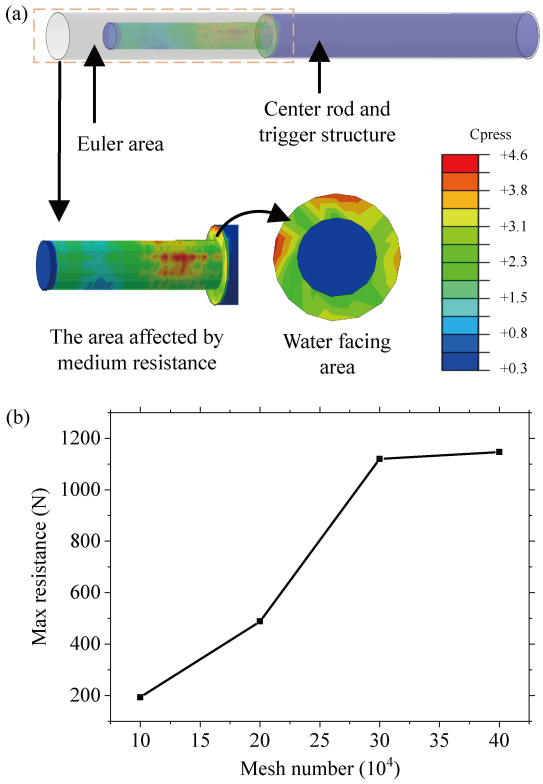

Fig. 6. Simulation results and grid independence verification: (a) Contact stress distribution from the simulation model and (b) grid independence test with a mesh containing 305,238 elements.

ing medium resistance, including initial pulling speed (related to pulling force), medium density, and object density. The specific experiments and their results are presented below.

3.2.1 Impact of initial pulling speed

The initial pulling speed and pulling force are related factors. Under the action of pulling force, the center rod has a preset stroke for accelerating the center rod, which then drives the trigger structure to move. During this process, the acceleration of the center rod and momentum transfer occur due to a collision between the center rod and the trigger structure. The specific process is shown in Figs. 2(d) and 2(e).

In the proposed coring tool, the mass of the center rod m_c is 4.8 kg, the mass of the trigger structure m_t is 20.2 kg (the combined mass of the two (m)) is 25 kg), the mass of the salvage tool (m_s) is 10 kg, and the preset acceleration stroke (x) is 200 mm. Assuming a non-destructive momentum transfer process between the center rod and the triggering structure with negligible duration, the relationship between the initial tension F_p and the combined velocity V' of the center rod and triggering structure can be obtained through the following formula:

$$\begin{cases} V^2 - V_0^2 = 2ax \\ (m_s + m_c + m_t)\,V' = (m_s + m_c)\,V \\ F_p - (m_c + m_s)\,g = (m_c + m_s)\,g \end{cases} \tag{2}$$

where V represents the state velocity before the momentum transfer of the center rod and the trigger structure, V_0 is 0 m/s, and V' denotes the common velocity after the momentum transfer.

$$V' = \frac{m_c + m_s}{m_c + m_t + m_s}\sqrt{2\left(\frac{F_p}{m_c + m_s} - g\right)x + V_0^2} \tag{3}$$

Because the salvage tool also needs to accelerate during the above process, a portion of the tension needs to be accelerated to the same speed as the center rod, and the magnitude of the force on both is positively correlated with the mass. For this purpose, F' can be taken as the tensile force acting on the center rod, satisfying the following formula:

$$F' = F_p - m_s\,(a + g) \tag{4}$$

Under the initial pulling force of 350 N ($F' = 250$ N can be obtained according to Eq. (4)), the pulling force can be balanced with the gravity of the fishing tool, center rod and trigger structure, and V' can reach 0.99 m/s in this state. To test the sensitivity of medium resistance to velocity, simulation calculations were first conducted for medium resistance under the condition of an initial pulling force of 350 N, with a speed variation range from 0.1 to 1.0 m/s. By setting the corresponding F' and V' in the simulation model, the velocity change curve of the measuring point can be obtained under the same setting, as shown in Fig. 7.

The experimental results depicted in Fig. 7 reveal that, across various initial velocities, the maximum medium resistance occurs within an extremely brief contact duration, reaching the millisecond scale. Over time, a discernible diminishing trend in velocity can be observed, signifying a substantial medium force in the form of resistance that impedes the object's continuous motion. Furthermore, as speed increases, the maximum acceleration induced by the medium resistance exhibits proportional growth. The resistance of the medium displays temporal fluctuations, primarily attributed to the constrained internal space. The liquid medium undergoes oscillations within this confined space, leading to variations in acceleration. However, in a broader context, it is the force that acts as an impediment to movement, a trend further supported by the observed changes in speed.

Based on the experimental findings depicted in Fig. 8(a), it is evident that as the speed escalates, the maximum medium resistance demonstrates a concurrent increase, with the rate of escalation intensifying progressively. It is noteworthy that within the low-speed range (< 0.4 m/s), the resistance of the liquid medium is comparatively minimal. Within the velocity spectrum of 0.4 to 2 m/s, the velocity exerts a pronounced influence on the medium resistance. In the high-speed range (2-2.69 m/s), the medium resistance is still relatively high, whereas the sensitivity of medium resistance to velocity decreases, indicating that this phenomenon may be caused by spatial constraints inside the corer. Specifically, at an initial speed of 0.71 m/s and an initial pulling force of 250 N, the maximum medium resistance reaches 1,179 N.

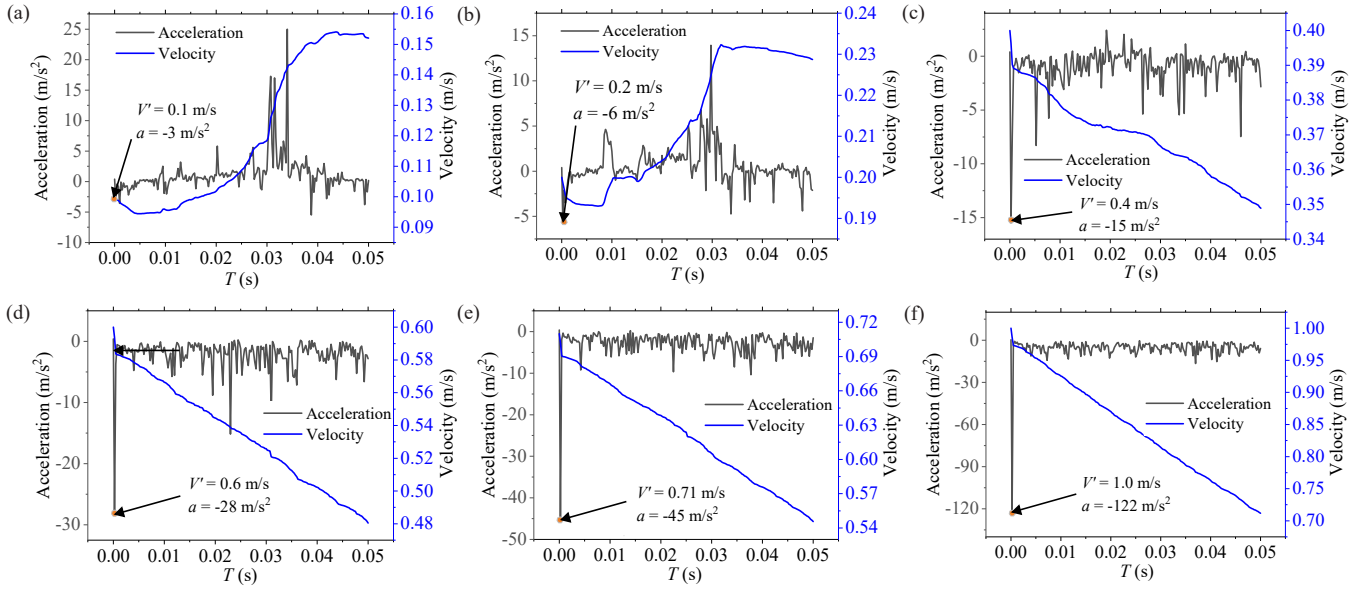

Fig. 7. Variation in velocity and acceleration under different initial velocities V': (a) 0.1, (b) 0.2, (c) 0.4, (d) 0.6, (e) 0.71 and (f) 1.0 m/s.

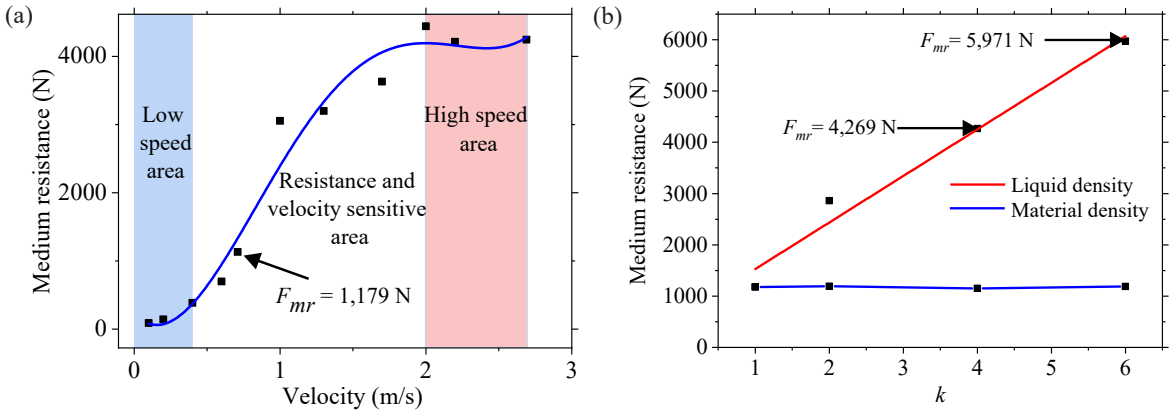

Fig. 8. Simulation analysis of medium resistance: (a) Velocity-dependent curve of maximum medium resistance under initial tension ($F' = 250$ N) and (b) effect of liquid density ρ_l and material density ρ_m on resistance.

Table 2. Influence of liquid density and object density on resistance.

k	ρ_m (kg/m^3)	F_{mr1} (N)	ρ_l (kg/m^3)	F_{mr2} (N)
1	8,000	1,179	1,000	1,179
2	16,000	1,190	2,000	2,861
4	32,000	1,150	4,000	4,269
6	48,000	1,189	6,000	5,971

Notes: F_{mr1} indicates modifying only the density of the metal material, while F_{mr2} refers to modifying only the density of the liquid medium.

3.2.2 Influence of medium density and object density

During the experiment, the initial density of the liquid medium is $\rho_l = 1{,}000$ kg/m^3. With an initial density of 304 grade material $\rho_m = 8{,}000$ kg/m^3, the density properties of the material can be directly modified to consider the impact of different densities on the resistance of liquid media. Therefore, we set the density of the liquid medium to k times ρ_l, where k can take values from the set [1, 2, 4, 6]. Similarly, the density of the 304 grade material is also scaled by a factor of k times ρ_m, with parameter values chosen from [1, 2, 4, 6]. All other experimental settings remain consistent with the preceding experiments.

From Table 2, it is evident that the density of the medium exhibits a linear relationship with the magnitude of liquid resistance, increasing with density. At the initial velocity V', with the standard density of water ($\rho_l = 1{,}000$ kg/m^3) measuring 0.71 m/s, the medium resistance F_{mr} is 1,179 N. At a density six times that of water, the medium resistance can reach 5,971 N, as shown in Fig. 8(b). Regarding the density of the object, i.e., the center rod and trigger structure, the acceleration decreases with increasing object density. However, due to the density increase, the magnitude of the medium resistance obtained from the formula $F = ma$ does not change

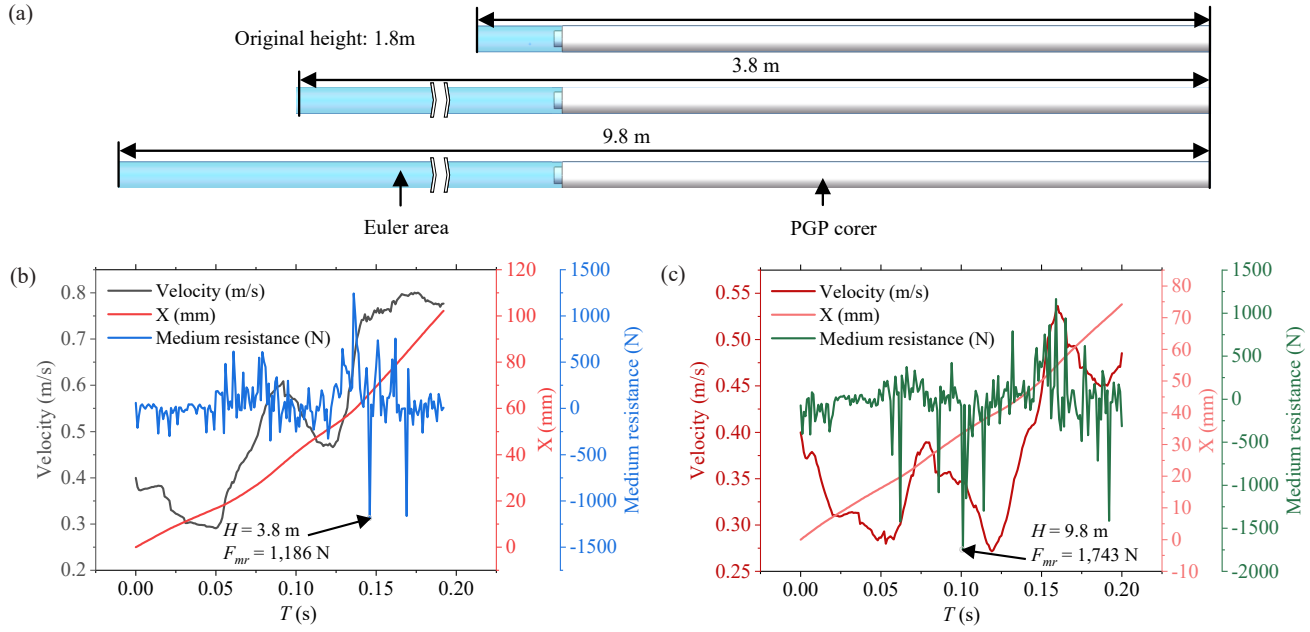

Fig. 9. Testing results at varying water depths: (a) Initial water depth of 1.8 m, with tests extended to depths of 3.8 and 9.8 m, (b) velocity, displacement, and resistance curves at a depth of 3.8 m and (c) 9.8 m.

significantly and remains around 1,179 N, fluctuating by 3%. Therefore, it can be considered that the density of an object is not significantly related to the resistance generated by the medium.

3.2.3 Influence of water depth

As the horizontal depth increases, the drilling trajectory is increasingly influenced by gravity, leading to a proportional increase in the distance from the wellhead at the completion of drilling. Consequently, a substantial accumulation of drilling fluid and coal shavings mixture occurs at this time. This results in an extended distance; in addition, the drilling fluid environment introduces a notable liquid resistance, impeding the success rate of pressure-preserved core sampling. To address this issue, we conducted simulations by extending the length of the Euler region, varying it between 3.8 and 9.8 m while keeping the initial model's Euler region length at 1.8 m, as depicted in Fig. 9(a). The primary consideration for selecting a depth of 1.8 m was to ensure that the coring device can be fully submerged in the water environment. The selection of water depths of 3.8 and 9.8 m was based on fitting the estimated water depths under on-site horizontal coring conditions of 60 and 120 m, respectively. Building upon the insights gained from previous experiments, this study set an initial tension of 300 N and an initial velocity of 0.4 m/s.

The analysis of the simulation experiment results in Figs. 9(b) and 9(c) reveal that under the experimental condition of an initial velocity of 0.4 m/s, the maximum liquid resistance did not occur at the moment of contact, possibly due to the initial velocity being in the low-speed region. The formation of maximum resistance at this stage may require the superposition of multiple waves, which is consistent with the phenomena depicted in Figs. 7(a) and 7(b). In addition, the maximum resistance of liquid media is positively correlated with depth, reaching 1,186 N at a depth of 3.8 m and 1,743 N at a depth of 9.8 m. This observation emphasizes the substantive relationship between liquid depth and resistance, highlighting the critical impact of depth on hydraulic resistance encountered during drilling operations.

3.3 Shear strength calculation and optimal design scheme

The earlier analysis delved into the factors influencing the resistance of liquid media, primarily encompassing initial pulling force F_p, initial pulling speed V', medium density ρ_l, and object density ρ_m. Among these, the initial pulling force is a predetermined parameter set to balance the reaction forces experienced by the system during the pulling process, including gravity and medium resistance (the focal point of this study). The initial velocity and initial pulling force form a correlated pair of variables. With the mass determined, a larger initial pulling force corresponds to a greater initial velocity. The density of the medium also amplifies the resistance of the liquid, with a linear relationship between the two. The density of objects has a minimal effect, which phenomenon appears to be intrinsically linked to the internal structural design of the proposed PGP corer. Initially, the swift motion of the triggering mechanism induces the formation of an internal cavity at the coring bit's end. Concurrently, the constricted flow channels impede the timely replenishment of this cavity by the surrounding water, resulting in a disproportionately higher pressure at the upper end of the triggering structure compared to its lower end. Moreover, the rapid acceleration of the triggering structure prevents the prompt expulsion of incompressible water from the upper end and the internal cavity of the PGP corer, significantly increasing the resistance of

the liquid medium. Thus, during the initial acceleration phase, the combined effects of these dynamics generate substantial resistance.

In the practical context of coal mining coring, horizontal holes predominantly assume a downward orientation. When the horizontal hole depth surpasses 60 m, the vertical depth can extend to 3 m (Ma et al., 2022). Typically, these holes contain a significant volume of drilling fluid, intensifying the resistance impact of the triggering component in the vertical direction, primarily attributable to liquid-induced resistance. In this scenario, the pulling triggering force F_p must adhere to the following formula:

$$F_p = (m_s + m_c + m_t)(g + a) + F_{mr} \tag{5}$$

According to the shear force balance relationship of the shear pin, the calculation formula for the allowable lateral force F_l of the pin can be obtained, which satisfies the following relationship:

$$F_l = \frac{\tau_p \pi d^2 Z}{4} \geq F_p S \tag{6}$$

where τ_p stands for the required shear stress for the pin. For commonly used materials of the pin, this paper takes $\tau_p = 80$ MPa; d represents the diameter of the pin, in millimeters; Z denotes the number of shear surfaces of the shear pin; S is the safety factor

In the previous design, the shear pin parameters were set as follows: $Z = 1$, aluminum material with a shear strength of 80 MPa, and a pin diameter $d = 3$ mm. The safety factor S was chosen as 1.5, as referenced in Sukumar et al. (2020). The calculated allowable lateral shear force F_l was 565.2 N, which is significantly smaller than the resistance of 1,179 N under the initial pulling speed of 0.71 m/s.

Under the initial tensile force of 350 N, the remote trigger operation of the tool can be achieved without considering the resistance of the medium. However, in actual underground operations, the downward hole and the water storage inside this hole will inevitably have a significant impact on the triggering action due to medium resistance, leading to triggering failure. Moreover, as the initial tension increases, the initial velocity will also rise, along with the resistance of the medium. The increase in initial tension may reach the safety threshold of the allowable shear strength of the shear breaker, resulting in triggering failure. Furthermore, it becomes challenging to determine the success of core extraction at the wellhead, affecting the stability of core extraction and causing a workload of repeated core extraction.

In light of the aforementioned results, it is recommended to commence with a slower initial pulling speed and incrementally increase the pulling force in a gradual manner. This approach ensures that the trigger structure reaches the designated position, facilitating the successful closure of the pressure-preserved controller. Subsequently, the tension can be further increased, the shear pin can be cut, and the entire remote trigger process can be completed. Furthermore, building upon the aforementioned analysis and taking into account a maximum immersion depth of 9.8 m, the estimated magnitude of medium resistance is 1,750 N. Considering a safety factor of 1.5, the required force that the pin should withstand is determined to be 3,150 N. For the selected pin material, an aluminum-magnesium alloy with a diameter of 4 mm and a shear strength ranging from 130-160 MPa is chosen. The minimum design value is set to 130 MPa and Z is set to 2. Employing Eq. (6), the calculated allowable shear force is established at 3,266 N, surpassing the required 3,150 N and satisfying the stipulated usage criteria.

3.4 Remote triggering test considering liquid resistance

The main purpose of simulation is to quantitatively determine the magnitude of the resistance of the liquid medium, providing theoretical support for the selection of parts for the PGP-Coring tool. To verify the correctness of the simulation results, remote triggering tests of PGP-Coring tool were conducted at the Tangshan experimental base. A JS-2000A rope winch was used as a constant speed trigger power source, with a winch motor power of 7.5 kW, first speed of 0.43 m/s, and second speed of 0.9 m/s. The available sizes for shear pins were 2 to 5 mm, with 2 shear surfaces and a shear strength of 130 MPa. The diameter selection of the pin can be obtained using Eq. (7), and the calculation result of d should be rounded up to meet the size requirements. On the basis of calculation, this type of pin can meet the requirement of enabling the remote triggering structure to reach the winch speed within a short distance; hence, it can be considered that the triggering structure moves at a constant speed at the winch speed. We conducted remote triggering experiments under two media (air and water) and two triggering speed conditions, and judged whether the calculation met the set requirements by observing whether the pin was cut at the specified position.

$$\begin{aligned} d &= \left\lceil \sqrt{\frac{4F_p S}{\tau_p \pi Z}} \right\rceil \\ &= \left\lceil \sqrt{\frac{4S}{\tau_p \pi Z}\left[(m_s + m_c + m_t)(g + a) + F_{mr}\right]} \right\rceil \end{aligned} \tag{7}$$

As shown in Table 3, under the condition of air medium, the influence of medium resistance is negligible. The main consideration is the gravity of the remote triggering structure, which means that the required tensile force F_p is less than F_l/S. Under water medium conditions, with a water depth of 1.8 m and a triggering speed of 0.43 m/s, although the shear strength of the 2-mm pin can meet the requirement of overcoming gravity, it still fails to trigger successfully multiple times in the experiment. When the diameter of the pin is increased to 3 mm, triggering can be completed. Based on the fitting curve in Fig. 8(a), we predicted the liquid medium resistance at this speed and added the data to the pin strength calculation formula. In this case, the maximum pulling force F_l/S that the pin can provide is greater than the required pulling force F_p, thus triggering the experiment successfully. As the speed further increases to 0.9 m/s, considering the water medium resistance condition of 2,170 N, a pin with a diameter of 5 mm is selected for testing, which can successfully achieve remote triggering. The above results fully verify the correctness of

Table 3. Remote triggering test of PGP-Coring tool conducted at Tangshan experimental base.

V (m/s)	Without fluid resistance					With fluid resistance				
	F_{mr} (N)	F_p (N)	F_l/S (N)	d (mm)	Result	F_{mr} (N)	F_p (N)	F_l/S (N)	d (mm)	Result
0.43 (air)	0	392	544	2	Y	0	392	1,225	3	Y
0.43 (water)	0	392	544	2	N	455	847	1,225	3	Y
0.9 (water)	0	392	544	2	N	2,170	2,562	3,402	5	Y

Notes: Y represents successful remote triggering, while N represents failed triggering.

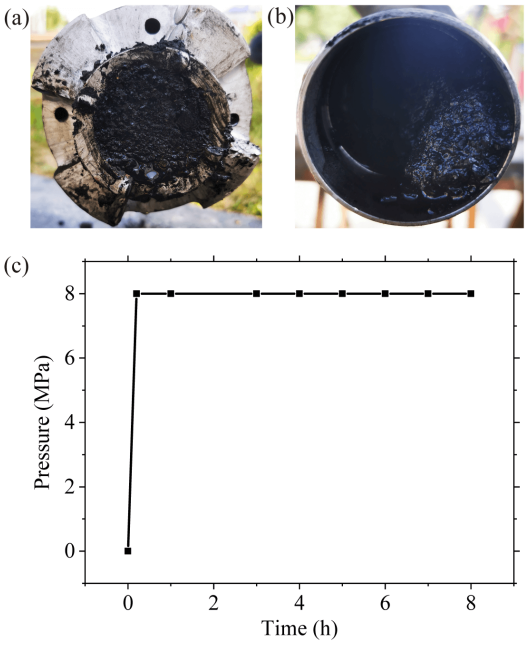

Fig. 10. Laboratory coring tests: (a) Filling the coring bit with coal powder, (b) obtained coal sample and (c) 8-hour pressure preservation test.

the simulation results and the importance of pin selection, while they also indicate that the medium resistance in water environment cannot be ignored.

4. Experiments

4.1 Laboratory coring tests

In order to ensure the effectiveness of the proposed equipment, a horizontal pull-out test of the corer was first conducted at the coring experimental base to verify whether the pull-out under normal air medium conditions is normal and whether the normal pressure-preserved closure triggering process can be achieved. Subsequently, horizontal simulation core testing was performed. The process of obtaining coal samples was simulated by filling coal powder at the terminal end, and the pressure-preserved mechanism was activated using a remote triggering device, as shown in Fig. 10(a). The coal samples retrieved from the core tube are illustrated in Fig. 10(b).

In order to ensure the effectiveness of the proposed equipment, a horizontal pull-out test of the corer was first conducted at the coring experimental base to verify whether the pull-out under normal air medium conditions is normal and whether the normal pressure-preserved closure triggering process can be achieved. Subsequently, horizontal simulation core testing was performed. The process of obtaining coal samples was simulated by filling coal powder at the terminal end, and the pressure-preserved mechanism was activated using a remote triggering device, as shown in Fig. 10(a). The coal samples retrieved from the core tube are illustrated in Fig. 10(b).

Next, to meet on-site requirements for pressure-bearing capacity, we conducted a long-term stable pressure test on the PGP corer under 8 MPa conditions after completing the triggering action. During the test, no leakage was found and the pressure could be effectively maintained. The results are shown in Fig. 10(c). This device is designed to obtain authentic samples for deep coal mines, and its pressure-bearing capacity determines the allowable pressure level of the *in-situ* environment. The greater the pressure-bearing capacity, the more suitable the device is for deeper coal seams. This is because the integrity of the sample can only be preserved by maintaining its *in-situ* pressure environment, avoiding the internal gas escape of the sample and thus improving the measurement accuracy of coal seam parameters.

Next, to meet on-site requirements for pressure-bearing capacity, we conducted a long-term stable pressure test on the PGP corer under 8 MPa conditions after completing the triggering action. During the test, no leakage was found and the pressure could be effectively maintained. The results are shown in Fig. 10(c). This device is designed to obtain authentic samples for deep coal mines, and its pressure-bearing capacity determines the allowable pressure level of the *in-situ* environment. The greater the pressure-bearing capacity, the more suitable the device is for deeper coal seams. This is because the integrity of the sample can only be preserved by maintaining its *in-situ* pressure environment, avoiding the internal gas escape of the sample and thus improving the measurement accuracy of coal seam parameters.

4.2 Field tests

To further verify the reliability of the calculation, underground field core testing was conducted at Chengzhuang Mine in Jincheng City, Shanxi Province. The roadway of the testing site is approximately 700 m underground, with a maximum horizontal core hole depth of about 120 m and a vertical height variation of up to 10 m between the core-taking point and the hole. The core extraction process is detailed in Section 2.2.

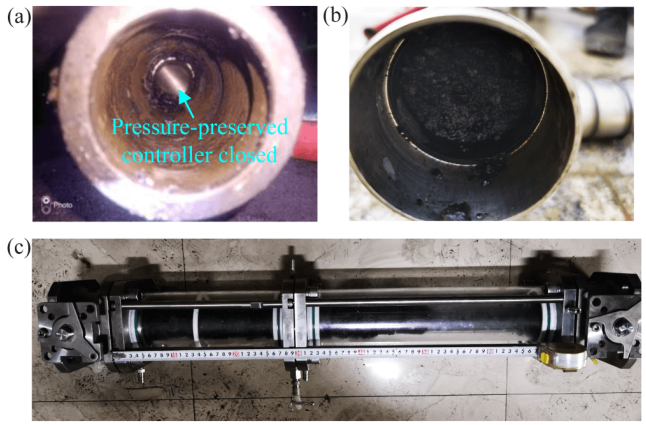

Fig. 11. Photograph of the field coring test: (a) Pressure-preserved controller successfully sealed, (b) coal samples retained within the core barrel and (c) an obtained coal sample with a length of 500 mm.

With the recommended pin size, the pressure-preserved controller successfully sealed, allowing for the extraction of a coal sample with its pressure- and gas- preserved. Among the captured underground images, Fig. 11(a) shows the pressure-preserved controller at the lower end of the PGP corer achieving complete closure; Fig. 11(b) illustrates the coal sample securely retained within the core barrel after extraction, confirming the successful acquisition of pressure- and gas-preserved coal samples; finally, Fig. 11(c) presents the obtained coal sample, measuring 500 mm in length.

With the recommended pin size, the pressure-preserved controller successfully sealed, allowing for the extraction of a coal sample with its pressure- and gas-preserved. Among the captured underground images, Fig. 11(a) shows the pressure-preserved controller at the lower end of the PGP corer achieving complete closure; Fig. 11(b) illustrates the coal sample securely retained within the core barrel after extraction, confirming the successful acquisition of pressure- and gas-preserved coal samples; finally, Fig. 11(c) presents the obtained coal sample, measuring 500 mm in length.

5. Conclusions

Deep coal mines contain vast resources, yet the accurate measurement of parameters of coal seams for reserve assessment remains challenging. The primary difficulty lies in retrieving authentic samples that preserve the *in-situ* environment and provide reliable evaluation for metrics such as gas content. This article addresses these challenges and offers the following contributions:

1) A remotely triggered PGP-Coring tool is presented, that is specifically designed for deep coal mines to minimize gas leakage during sample transportation, thereby improving the reliability of gas content measurements. The proposed tool can extract coal seam samples with a diameter of 50 mm from complex *in-situ* environments, maintaining environmental pressure to ensure sample integrity.
2) To enhance the stability of remote triggering in deep *in-situ* environments, the impact of medium resistance on the triggering process is analyzed through CEL simulation. Based on these insights, a triggering force verification formula that accounts for medium resistance is proposed, along with optimized core parameters for the PGP-Coring tool, including initial tension, traction speed, and shear pin strength.
3) Laboratory experiments validated the stability of remote triggering and the pressure-bearing capability of the PGP-Coring tool. Furthermore, on-site tests successfully obtained pressure- and gas preserved coal samples, demonstrating the tool's effectiveness under real conditions.

However, the proposed tool requires transporting pressure-preserved coal samples to a ground laboratory for complete measurements, leading to extended processing times. In future work, we aim to facilitate direct gas content measurement underground, making the tool more suitable for multi-point gas content assessments in coal mines.

Acknowledgements

The authors are grateful for the financial support from the National Natural Science Foundation of China (No.51827901), the China Postdoctoral Science Foundation (No. 2023M742446), and the National Natural Science Foundation of China (Nos. 52104096 and 42477190).

Conflict of interest

The authors declare no competing interest.

References

Abid, K., Spagnoli, G., Teodoriu, C., et al. Review of pressure coring systems for offshore gas hydrates research. Underwater Technology, 2015, 33(1): 19-30.

Abegg, F., Hohnberg, H. J., Pape, T., et al. Development and application of pressure-core-sampling systems for the investigation of gas-and gas-hydrate-bearing sediments. Deep Sea Research Part I: Oceanographic Research Papers, 2008, 55(11): 1590-1599.

Baouche, R., Wood, D. A. Characterization and estimation of gas-bearing properties of Devonian coals using well log data from five Illizi basin wells (Algeria). Advances in Geo-Energy Research, 2020, 4(4): 356-371.

Bertard, C., Bruyet, B., Gunther, J. Determination of desorbable gas concentration of coal (direct method). International Journal of Rock Mechanics and Mining Sciences & Geomechanics Abstracts, 1970, 7(1): 43-65.

Diamond, W. P., Schatzel, S. J. Measuring the gas content of coal: A review. International Journal of Coal Geology, 1998, 35(1-4): 311-331.

Dickens, G. R., Paull, C. K., Wallace, P. Direct measurement of in situ methane quantities in a large gas-hydrate reservoir. Nature, 1997, 385(6615): 426-428.

Dickens, G. R., Schroeder, D., Hinrichs, K. U. The pressure

core sampler (PCS) on ODP Leg 201: General operations and gas release. In Proceedings of the ocean drilling program, Initial Reports, 2003, 201: 1-22.

Guo, D., Xie, H., Gao, M., et al. *In-situ* pressure-preserved coring for deep oil and gas exploration: Design scheme for a coring tool and research on the *in-situ* pressure-preserving mechanism. Energy, 2024, 286: 129519.

He, S., Peng, Y., Jin, Y., et al. Review and analysis of key techniques in marine sediment sampling. Chinese Journal of Mechanical Engineering, 2020, 33: 160-176.

Huang, W., Li, J., Liu, Z., et al. Study of a low-disturbance pressure-preserving corer and its coring performance in deep coalmining conditions. International Journal of Mining Science and Technology, 2023, 33(11): 1397-1410.

Kvenvolden, K. A., Cameron, D. Pressure core barrel; application to the study of gas hydrates, deep sea drilling project site 533, leg 76. Initial Reports of the DSDP, 1983, 76: 367-375.

Li, C., Xie, H., Gao, M., et al. Novel designs of pressure controllers to enhance the upper pressure limit for gas-hydrate-bearing sediment sampling. Energy, 2021, 227: 120405.

Li, J., Lu, S., Zhang, P., et al. Estimation of gas-in-place content in coal and shale reservoirs: A process analysis method and its preliminary application. Fuel, 2020, 259: 116266.

Li, J., Wang, J., Hu, Y., et al. Contact performance analysis of pressure controller's sealing interface in deep *in-situ* pressure-preserved coring system. Petroleum Science, 2022, 19(3): 1334-1346.

Li, L., Sun, Z., Wang, F., et al. Study on the gas desorption law and indicator influencing factors of fixed-size coal samples. Scientific Reports, 2019a, 9(1): 17134.

Li, X., Zhang, Y., Wang, H., et al. Design and trial-manufacture of the pressure-holding core drilling tool for evaluation of coal-seam gas. Geology and Exploration, 2019b, 55(4): 1045-1050 (in Chinese).

Li, X., Zhang, X., Ma, Y., et al. Design and Experimental Study of an Improved Pressure Core Sampler for Marine Gas Hydrates. ACS omega, 2024, 9(13): 14977-14984.

Ma, H., Chen, S., Xue, D., et al. Outlook for the coal industry and new coal production technologies. Advances in Geo-Energy Research, 2021, 5(2): 119-120.

Mahmoud, H., Hamza, A., Nasser, M. S., et al. Hole cleaning and drilling fluid sweeps in horizontal and deviated wells: Comprehensive review. Journal of Petroleum Science and Engineering, 2020, 186: 106748.

Masayuki, K., Satoru, U., Masato, Y. Pressure temperature core sampler (ptcs). Journal of the Japanese Association for Petroleum Technology, 2006, 71(1): 139-147.

Ma, T., Liu, J., Fu, J., et al. Drilling and completion technologies of coalbed methane exploitation: an overview. International Journal of Coal Science & Technology, 2022, 9(1): 68.

Pape, T., Hohnberg, H. J., Wunsch, D., et al. Design and deployment of autoclave pressure vessels for the portable deep-sea drill rig MeBo (Meeresboden-Bohrgerät). Scientific Drilling, 2017, 23: 29-37.

Saghafi, A. Discussion on determination of gas content of coal and uncertainties of measurement. International Journal of Mining Science and Technology, 2017, 27(5): 741-748.

Schultheiss, P., Francis, T., Holland, M., et al. Pressure coring, logging and subsampling with the hyacinth system. Geological Society, London, Special Publications, 2006, 267(1): 151-163.

Schultheiss, P., Holland, M., Humphrey, G. Wireline coring and analysis under pressure: Recent use and future developments of the hyacinth system. Scientific Drilling, 2009, 7: 44-50.

Sukumar, T., Ramesh Bapu, B., Durga Prasad, B. Prediction of hyperelastic material sealing pressure using experimental and numerical analyses. Journal of Elastomers & Plastics, 2020, 52(8): 717-727.

Sun, S., Zhang, Q., Zheng, K., et al. Technology and equipment of sealed coring for accurate determination of coalbed gas content in ground well. Journal of China Coal Society, 2020, 45(7): 2523-2530 (in Chinese).

Wang, Z., Tang, X., Yue, G., et al. Physical simulation of temperature influence on methane sorption and kinetics in coal: Benefits of temperature under 273.15 k. Fuel, 2015, 158: 207-216.

Xie, H., Gao, M., Zhang, R., et al. Application prospects of deep *in-situ* condition-preserved coring and testing systems. Advances in Geo-Energy Research, 2024, 14(1): 12-24.

Xie, H., Hu, Y., Gao, M., et al. Research progress and application of deep *in-situ* condition preserved coring and testing. International Journal of Mining Science and Technology, 2023, 33(11): 1319-1337.

Yang, L., Su, Y., Luo, J., et al. Development and application of gw-cp194-80a pressure-maintaining coring tool. Natural Gas Industry, 2020, 40(4): 91-96 (in Chinese).

Yee, D., Seidle, J. P., Hanson, W. B. Gas sorption on coal and measurement of gas content: Chapter 9, in SG 38: Hydrocarbons from Coal, edited by B. E. Law and D. D. Rice, American Association of Petroleum Geologists, Boulder, Tulsa, pp. 203-218, 1993.

Zhu, Q., Su, X., Yang, L., et al. Development and field test of gw-cp194-80m cbm dual pressure coring tool. Special Oil and Gas Reservoirs, 2020, 27(5): 139-144. (in Chinese)